

Auto-oscillations in YIG/Pt microstructures driven by the spin Seebeck effect

V. Lauer,¹ M. Schneider,¹ T. Meyer,¹ C. Dubs,² P. Pirro,¹ T. Brächer,³ F. Heussner,¹ B. Lägél,¹ V. I. Vasyuchka,¹ A. A. Serga,¹ B. Hillebrands,¹ and A. V. Chumak¹

¹*Fachbereich Physik and Landesforschungszentrum OPTIMAS, Technische Universität Kaiserslautern, 67663 Kaiserslautern, Germany*

²*INNOVENT e.V., Technologieentwicklung, Prüssingstraße 27B, 07745 Jena, Germany*

³*SPINTEC, UMR-8191, CEA-INAC/CNRS/UJF-Grenoble/Grenoble-INP, 17 Rue des Martyrs, 38054 Grenoble, France*

(Dated: 22 December 2016)

We demonstrate experimentally that a thermal gradient in a nanostructured YIG(66 nm)/Pt(7 nm) bilayer can trigger coherent spin dynamics in the YIG layer due to a spin Seebeck effect (SSE) induced spin-transfer torque (STT). The experiment is performed on a 4 μm long and 475 nm wide YIG/Pt nanowire at room temperature. Magnetization precession is excited by applying 50 ns long dc pulses to the structure, and detected using Brillouin light scattering (BLS) spectroscopy. SSE-driven magnetization auto-oscillations appear on a short time scale of around 20 ns, afterwards the BLS signal decays again. The observed behavior is caused by the interplay of the SSE, which depends on the thermal gradient, with effects depending on the absolute temperature, e.g., the spin mixing conductance. Numerical simulations show that the thermal gradient saturates within a few nanoseconds, but the absolute temperature of the system steady increases during the dc pulse. Moreover, the experimental data demonstrate a small contribution from the spin Hall effect. Our findings suggest the generation of a coherent precession state from incoherent SSE-injected magnons and reveal an application potential for microwave sources at room temperature.

Spin-transfer torque (STT)¹ caused by the injection of spin-polarized electrons into magnetic structures has attracted attention due to the potential realization of efficient microwave sources² and magnonic components with compensated spin-wave losses³. The generation of spin-polarized currents based on the spin Hall effect (SHE)⁴ is of particular importance since it does not require a charge current to pass through the magnetic material. Therefore, it provides access to the application of STT to insulators such as yttrium iron garnet (YIG)^{3,5}. Partial compensation of the spin-wave damping^{6,7} and excitation of magnetization auto-oscillations^{8,9} in YIG/Pt bilayers by applying a dc current to the adjacent Pt layer were demonstrated recently. The spin Seebeck effect (SSE)^{10–12} is another method of spin-current generation which utilizes a thermal gradient rather than a charge current. This phenomenon might be of particular practical benefit since it potentially does not require a separate energy source, but could use parasitic heat sources that already exist in the system (e.g. such a component can be installed between a processor and a cooling element). There have been experimental studies showing that the spin current due to a heat gradient can apply a STT to a magnetic film resulting in the partial compensation of the spin-wave damping in YIG (as e.g. in Ref.¹³). Furthermore, first experimental evidences of SSE-excited magnetization precession in YIG/Pt nanowires at low temperatures investigated by means of electrical measurements have been recently reported¹⁴.

In this Letter, we show the experimental observation of magnetization auto-oscillations in the YIG layer of a YIG/Pt nanowire driven by dc pulses applied to the Pt

layer. Time-resolved microfocused Brillouin light scattering (BLS) spectroscopy¹⁵ is used to investigate the temporal evolution and the spatial distribution of the excited magnetization dynamics in the nanostructure. The experimental results show that the spin Seebeck effect is the main driving force behind the auto-oscillations. The particular nanostructure is shown in Fig. 1(b). Joule heating by the current pulses leads to an increase in the Pt temperature, and, consequently, to the formation of a thermal gradient across the YIG/Pt interface. The thermal gradient gives rise to a SSE-induced spin current injected into the YIG layer which exerts an anti-damping torque on the magnetization and, eventually, excites magnetization precession. The influence of the SHE-induced spin current is detected as well, but plays only a minor role in our experiments. Figure 1(a) schematically

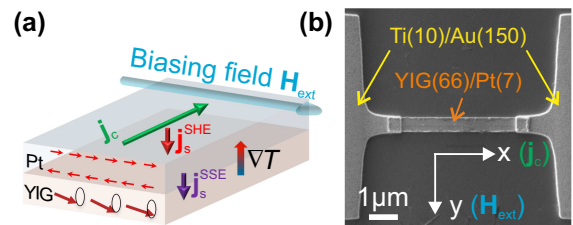


FIG. 1. (color online) (a) Illustration of the spin current generated by the SHE and by the SSE (due to a temperature gradient) in a YIG/Pt bilayer, if a charge current is passed through the Pt layer. (b) SEM image of a YIG/Pt nanowire connected to Ti/Au leads. The biasing field is along the y -direction, the charge current is along the x -direction.

shows the investigated YIG/Pt bilayer, indicating the directions of the externally applied biasing field \mathbf{H}_{ext} , the applied charge current density \mathbf{j}_c , the generated spin current density $\mathbf{j}_s^{\text{SHE}}$ due to the SHE, and the SSE-induced spin current density $\mathbf{j}_s^{\text{SSE}}$ due to the thermal gradient ∇T .

Figure 1(b) shows an exemplary SEM image of the investigated YIG/Pt nanowire and the Ti/Au structures (left and right) which are used as leads to apply the dc pulses. The nanowire is 475 nm wide and the distance between the leads is 4 μm . The structures were fabricated by growing a YIG film of 66 nm thickness by means of liquid phase epitaxy on a gadolinium gallium garnet (GGG) substrate¹⁶. Standard microwave-based ferromagnetic resonance (FMR) measurements yield a Gilbert damping parameter of $\alpha_{\text{YIG}} = 1.8 \times 10^{-4}$ for the bare YIG film. Next, plasma-assisted cleaning was used to remove potential contaminations before the sample was transferred into a molecular beam epitaxy (MBE) facility for the deposition of a 7 nm thick Pt layer on top of the YIG film. The deposited Pt layer was found to increase the Gilbert damping to $\alpha_{\text{YIG/Pt}} = 1.2 \times 10^{-3}$. The subsequent structuring of the YIG/Pt nanowires was achieved by electron-beam lithography and argon-ion milling. The leads (10 nm Ti and 150 nm Au) were patterned by using electron-beam lithography and vapor deposition.

For the BLS measurements, a laser beam with a wavelength of 491 nm and a power of 2 mW is focused onto the nanostructure. The laser-spot size is approximately 400 nm in diameter. The intensity of the frequency shifted and backscattered light is proportional to the square of the dynamic magnetization component, i.e. the spin-wave intensity. An in-plane biasing field of $\mu_0 H_{\text{ext}} = 90 \text{ mT}$ is used to magnetize the nanowire perpendicular to its length (along the y -direction), and 50 ns long dc pulses with a repetition time of 500 ns are passed through the nanowire (along the x -direction). Such a configuration allows for the injection of a pure spin current into the YIG layer due to two effects, the SSE and the SHE. The origin of the SSE is Joule heating of the Pt layer which creates a thermal gradient from the colder YIG to the hotter Pt (see Fig. 1(a)). As a result, a pure spin current is injected into the YIG, which exerts an anti-damping spin torque. This SSE-induced spin torque, in particular, depends only on the thermal gradient regardless of the alignment between the magnetization orientation and the charge current direction. The situation is different for the SHE-generated spin current which reverses if the field polarity or the current direction is reversed. Thus, the SHE-driven STT can act as a damping or anti-damping torque, depending on the orientation of the magnetic field with respect to the charge current direction.

Figure 2 shows the maximum BLS intensity measured in the center of the nanowire during the dc pulse as a function of the applied current for both field and current polarities. It clearly reveals that the threshold-like onset of magnetization auto-oscillations for current densities higher than $|j_c| > 1.3 \times 10^{12} \text{ A/m}^2$ is independent

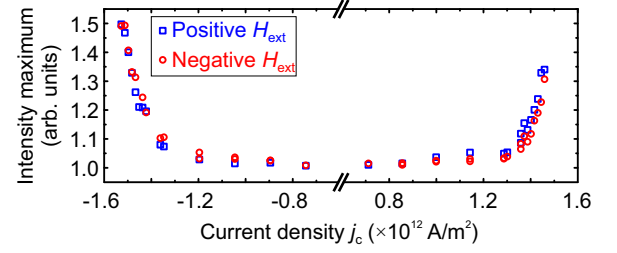


FIG. 2. (color online) BLS intensity maximum detected in the nanowire center during the applied dc pulse as a function of the current density. The threshold-like onset of auto-oscillations is observed for both magnetic field polarities and both current directions. The behavior is understood in terms of the SSE-generated anti-damping spin torque, accompanied by a weak contribution from the SHE.

of the field as well as of the current polarity. As already mentioned, this behavior can be understood by an anti-damping torque due to the SSE, but cannot originate from the SHE. However, the data points in Fig. 2 demonstrate a weak influence of the SHE-induced STT on the spin dynamics in accordance with theoretical expectations: The measured maximum BLS intensity is higher in the case of the additional anti-damping SHE-STT (blue squares (red circles) for $j_c > 0$ ($j_c < 0$) in Fig. 2). From the experimental data, it can be estimated that the SHE shifts the critical current density for the SSE-generated auto-oscillations in the nanowire under investigation by only 1%. We attribute the weak influence of the SHE in the nanowires to the relatively small spin-Hall angle due to the high quality Pt grown by means of MBE. It was recently reported that moderately dirty Pt layers grown by a sputtering technique yield up to 6 times larger spin-Hall angles compared to very clean growth processes¹⁷.

In the following, the temporal evolution of the SSE-generated auto-oscillations is addressed. In Fig. 3(a) the color-coded BLS-intensity is depicted as a function of the BLS frequency and time. Spin dynamics are excited during the applied dc pulse marked by the shaded area ($0 < t < 50 \text{ ns}$). Figure 3(b) shows the temporal behavior of the BLS frequency of the intensity maximum. Before the start of the dc pulse at $t < 0 \text{ ns}$, the system is in equilibrium and only thermal spin waves are observed at a frequency of 4.15 GHz. The BLS frequency then drops to approximately 4 GHz when the dc pulse is applied. Comparable frequency drops have been reported for auto-oscillations excited by the SHE-STT⁹. After the pulse has ended, i.e., at $t > 50 \text{ ns}$, the system slowly relaxes back to its original state. It should be noted that the spin dynamics at the lower frequency of 3.45 GHz are assumed to belong to some edge mode, which exists in the system permanently (not apparent from the color map) and has an intensity much lower than the thermal spin waves. The anti-damping STT during the pulse drastically increases the intensity of this particular mode as well. However, this mode is not in the focus of the

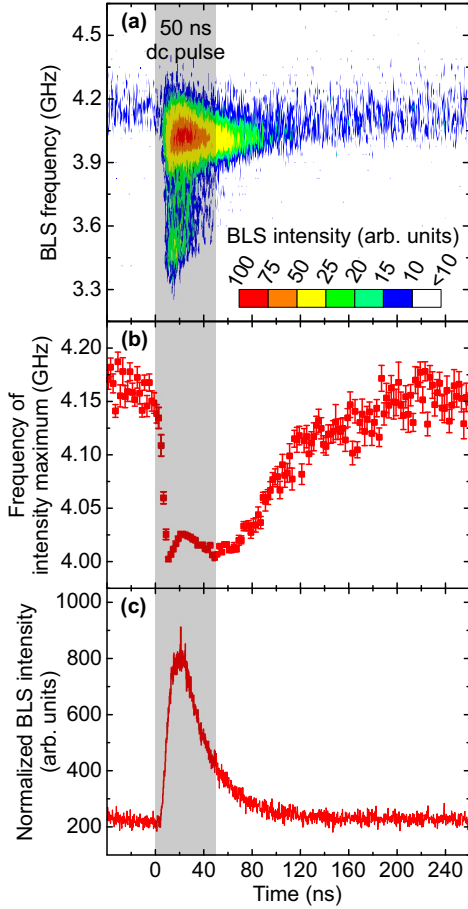


FIG. 3. (color online) (a) Color-coded BLS intensity as a function of the measured BLS frequency and time. The grayish area illustrates the duration of the 50 ns long dc pulse. (b) Temporal evolution of the BLS frequency of the intensity maximum. (c) Temporal evolution of the BLS intensity integrated over all measured BLS frequencies.

discussion in this Letter. A remarkable feature of SSE-generated auto-oscillations becomes apparent by analyzing the BLS intensity versus time, as shown in Fig. 3(c). Here, the intensity is integrated over all detected BLS frequencies from 3.0 GHz to 5.2 GHz. The BLS intensity clearly reaches a maximum within the first 20 ns and starts to decay before the end of the pulse. We contribute this behavior to the temporal evolution of the thermal gradient in combination with the overall heating of the nanostructure. According to numerical simulations (not shown here) using COMSOL Multiphysics®, the thermal gradient in the YIG layer rapidly increases and saturates within a few nanoseconds and, therefore, the SSE saturates as well. The overall temperature of the system, in contrast, steadily increases during the whole duration of the pulse. The temperature increase is assumed to decrease the spin-mixing conductance of the YIG/Pt interface¹⁸, and, therefore, the injected spin current drops, that is accompanied by the reduction of

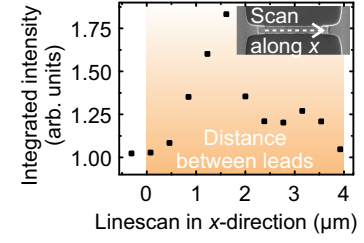


FIG. 4. (color online) Time- and frequency-integrated BLS intensity during the applied dc pulse as a function of the probing position along the nanowire. The orange-colored area illustrates the distance between the leads

the anti-damping torque. Such a drop of the BLS signal within the pulse duration (as shown in Fig. 3(c)) is observed for all tested current densities above the critical current density. However, our simplified picture may not necessarily be considered as complete. There are more temperature dependent parameters like, e.g., the spin diffusion length in the Pt layer and the magnon diffusion length in the YIG layer which could have a notable impact on the investigated processes. Also a decrease of the thermal gradient, e.g., due to the change of the thermal properties of the GGG substrate or due to the heating of the YIG layer by decaying spin waves, is not included in the simulations but has to be considered.

In order to display the spatial distribution of the auto-oscillations, a linescan in x -direction along the nanowire is performed. Figure 4 shows the frequency-integrated and time-integrated BLS intensity during the dc pulse as a function of the probing position. We detect the highest intensity in the center of the nanowire and observe an intensity drop close to the leads. This finding can be understood by the assumption that the metallic leads are significant better heat sinks than the YIG layer. Therefore, the temperature increase of the Pt layer is smaller closer to the leads, and, thus, also the thermal gradient at the YIG/Pt interface and the corresponding anti-damping torque is smaller close to the leads. This statement is well supported by the results of the numerical simulation. We believe that this is the reason why SSE-driven auto-oscillations were not observed in YIG/Pt microstructures widely covered by heat absorbing leads, as it is e.g. the case in the experiments of Refs.^{8,9,19}.

In conclusion, we demonstrate the generation of magnetization auto-oscillations in a YIG/Pt nanowire due to a thermal gradient. The SSE was identified as the origin for the anti-damping torque in the presented measurements. We observed a frequency drop of several hundred MHz during the excitation of spin dynamics. The temporal behavior of the BLS intensity, in particular the observation of a maximum followed by a decay within the dc pulse duration, could be attributed to the temporal behavior of the temperature distribution in the nanowire. Numerical simulations yield a fast saturation of the thermal gradient at the YIG/Pt interface, but a steady in-

crease of the absolute temperature in the system during the applied pulse. It was further shown that the onset of SSE-driven auto-oscillations appear only far away from the metal leads which act as optimal heat sinks. These findings are of great interest since they suggest the generation of a coherent precession state from incoherent SSE-injected magnons and reveal an application potential for the realization of microwave sources at room temperature.

ACKNOWLEDGMENTS

The authors thank G.E.W. Bauer for valuable discussions, and T. Löber for performing image acquisition shown in Fig. 1(b). This research has been supported by the EU-FET Grant InSpin 612759, by the ERC Starting Grant 678309 MagnonCircuits, and by the Deutsche Forschungsgemeinschaft (DU 1427/2-1, and SE 1771/4-2 within SPP 1538 "Spin Caloric Transport").

- ¹J.C. Slonczewski, *Current-driven excitation of magnetic multilayers*, J. Magn. Magn. Mater. **159**, L1-L7 (1996).
- ²A.N. Slavin, V.S. Tiberkevich, *Nonlinear auto-oscillator theory of microwave generation by spin-polarized current*, IEEE Trans. Magn. **45**, 1875-1918 (2009).
- ³A.V. Chumak, V.I. Vasyuchka, A.A. Serga, B. Hillebrands, *Magnon spintronics*, Nature Phys. **11**, 453 (2015).
- ⁴J.E. Hirsch, *Spin Hall effect*, Phys. Rev. Lett. **83**, 1834 (1999).
- ⁵Y. Kajiwara, K. Harii, S. Takahashi, J. Ohe, K. Uchida, M. Mizuguchi, H. Umezawa, H. Kawai, K. Ando, K. Takanashi, S. Maekawa, E. Saitoh, *Transmission of electrical signals by spin-wave interconversion in a magnetic insulator*, Nature **464**, 262-266 (2010).
- ⁶A. Hamadeh, O. d'Allivy Kelly, C. Hahn, H. Meley, R. Bernard, A.H. Molpeceres, V.V. Naletov, M. Viret, A. Anane, V. Cros, S.O. Demokritov, J.L. Prieto, M. Muñoz, G. de Loubens, O. Klein, *Full control of the spin-wave damping in a magnetic insulator using spin-orbit torque*, Phys. Rev. Lett. **113**, 197203 (2014).
- ⁷V. Lauer, D.A. Bozhko, T. Brächer, P. Pirro, V.I. Vasyuchka, A.A. Serga, M.B. Jungfleisch, M. Agrawal, Yu.V. Kobljanskyj, G.A. Melkov, C. Dubs, B. Hillebrands, A.V. Chumak, *Spin-transfer torque based damping control of parametrically excited spin waves in a magnetic insulator*, Appl. Phys. Lett. **108**, 012402 (2016).
- ⁸M. Collet, X. de Milly, O. d'Allivy Kelly, V.V. Naletov, R. Bernard, P. Bortolotti, J. Ben Youssef, V.E. Demidov, S.O. Demokritov, J.L. Prieto, M. Muñoz, V. Cros, A. Anane, G. de Loubens, O. Klein, *Generation of coherent spin-wave modes in yttrium iron garnet microdiscs by spin-orbit torque*, Nat. Commun. **7**, 10377 (2016).
- ⁹V.E. Demidov, M. Evelt, V. Bessonov, S.O. Demokritov, J.L. Prieto, M. Muñoz, J. Ben Youssef, V.V. Naletov, G. de Loubens, O. Klein, M. Collet, P. Bortolotti, V. Cros, A. Anane, *Direct observation of dynamic modes excited in a magnetic insulator by pure spin current*, Sci. Rep. **6**, 32781 (2016).
- ¹⁰K. Uchida, H. Adachi, T. Ota, H. Nakayama, S. Maekawa, E. Saitoh, *Observation of longitudinal spin-Seebeck effect in magnetic insulators*, Appl. Phys. Lett. **97**, 172505 (2010).
- ¹¹G.E.W. Bauer, E. Saitoh, B.J. van Wees, *Spin caloritronics*, Nat. Mater. **11**, 391-399 (2012).
- ¹²S.A. Bender, Y. Tserkovnyak, *Thermally driven spin torques in layered magnetic insulators*, Phys. Rev. B **93**, 064418 (2016).
- ¹³M.B. Jungfleisch, T. An, K. Ando, Y. Kajiwara, K. Uchida, V.I. Vasyuchka, A.V. Chumak, A.A. Serga, E. Saitoh, B. Hillebrands, *Heat-induced damping modification in yttrium iron garnet/platinum hetero-structures*, Appl. Phys. Lett. **102**, 062417 (2013).
- ¹⁴C. Safranski, I. Barsukov, H.K. Lee, T. Schneider, A.A. Jara, A. Smith, H. Chang, K. Lenz, J. Lindner, Y. Tserkovnyak, M. Wu, I.N. Krivorotov, *Spin caloritronic nano-oscillator*, arXiv:1611.00887 (2016).
- ¹⁵T. Sebastian, K. Schultheiss, B. Obry, B. Hillebrands, H. Schultheiss, *Micro-focused Brillouin light scattering: imaging spin waves at the nanoscale*, Front. Phys. **3**, 35 (2015).
- ¹⁶C. Dubs, O. Surzhenko, R. Linke, A. Danilewsky, U. Brückner, J. Dellith, *Sub-micrometer yttrium iron garnet LPE films with low ferromagnetic resonance losses*, arXiv:1608.08043 (2016).
- ¹⁷E. Sagasta, Y. Omori, M. Isasa, M. Gradhand, L.E. Hueso, Y. Niimi, Y. Otani, F. Casanova, *Tuning the spin Hall effect of Pt from the moderately dirty to the superclean regime*, Phys. Rev. B **94**, 060412(R) (2016).
- ¹⁸K. Uchida, T. Kikkawa, A. Miura, J. Shiomi, E. Saitoh, *Quantitative temperature dependence of longitudinal spin Seebeck effect at high temperatures*, Phys. Rev. X **4**, 041023 (2014).
- ¹⁹V. Lauer, M. Schneider, T. Meyer, T. Braeher, P. Pirro, B. Heinz, F. Heussner, B. Laegel, M.C. Onbasli, C.A. Ross, B. Hillebrands, A.V. Chumak, *Temporal evolution of auto-oscillations in a YIG/Pt microdisc driven by pulsed spin Hall effect-induced spin-transfer torque*, arXiv:1611.06054 (2016).